Current Research in Food Science 6 (2023) 100446

Contents lists available at ScienceDirect

Current Research in Food Science

journal homepage: www.sciencedirect.com/journal/current-research-in-food-science

Antidiabetic effects of protein hydrolysates from *Trachinotus ovatus* and identification and screening of peptides with α-amylase and DPP-IV inhibitory activities

Peng Wan [a,b,c], Bingna Cai [a,b], Hua Chen [a,b], Deke Chen [a,b], Xiangtan Zhao [a], Huabiao Yuan [a], Jingtong Huang [a], Xin Chen [d], Lianxiang Luo [e], Jianyu Pan [a,b,*]

[a] Key Laboratory of Tropical Marine Bio-resources and Ecology/Guangdong Key Laboratory of Marine Meteria Medica, South China Sea Institute of Oceanology, Chinese Academy of Sciences, Guangzhou, 510301, China
[b] Innovation Academy of South China Sea Ecology and Environmental Engineering (ISEE), Chinese Academy of Sciences, China
[c] Sanya Institute of Ocean Eco-Environmental Engineering, Sanya, 572000, China
[d] School of Environment and Chemical Engineering, Foshan University, Foshan, China
[e] The Marine Biomedical Research Institute, Guangdong Medical University, Zhanjiang, Guangdong, 524023, China

ARTICLE INFO

Handling Editor: Dr. Yeonhwa Park

Keywords:
Antidiabetic effects
Trachinotus ovatus
Protein hydrolysates
α-amylase
DPP-IV
Peptide identification and screening

ABSTRACT

In the present study, the antidiabetic properties of *Trachinotus ovatus* protein hydrolysates (TOH) in streptozotocin-induced diabetic mice were investigated, and peptides with α-amylase (AAM) and dipeptidyl peptidase IV (DPP-IV) inhibitory activities were identified and screened. The results showed that TOH alleviated body weight loss, polyphagia, blood glucose elevation and insulin secretion decline in diabetic mice. After 4 weeks of TOH administration, random blood glucose (RBG) decreased significantly. The TOH groups showed a dose-dependent reduction in fasting blood glucose (FBG), especially in the high-dose TOH group, which reduced FBG by 58% versus the effect of metformin. Moreover, TOH exerted a remarkable protective effect on hepatorenal function, as evidenced by increased superoxide dismutase (SOD), catalase (CAT) and glutathione peroxidase (GPX) and decreased serum urea levels. Histopathological studies confirmed that TOH can significantly protect the kidney and pancreas from histological changes, which was of great benefit for ensuring the normal secretion of insulin and preventing the occurrence of complications such as diabetic nephropathy. Two fractions with higher inhibitory activity against AAM and DPP-IV, F4 and F6, were obtained from the ultrafiltration of TOH-2 (≤3 kDa). A total of 19 potentially active peptides from F4 and 3 potentially active peptides from F6 were screened by LC–MS/MS combined with bioinformatic analysis. These peptides are small molecular peptides composed of 2–6 amino acids, rich in characteristic amino acids such as proline, arginine, phenylalanine and asparagine, and contain high proportions of peptides (68% for F4, 67% for F6) with hydrophobicity ≥50%. They offer potent antidiabetic potential and could potentially bind to the active sites in the internal cavities of the target enzymes AAM and DPP-IV. In summary, this study revealed for the first time the antidiabetic effects of protein hydrolysates of *Trachinotus ovatus* and their derived peptides, which are promising natural ingredients with the potential to be used for the treatment or prevention of diabetes.

1. Introduction

Diabetes mellitus is a serious and complex chronic metabolic disease characterized by elevated blood glucose levels due to insulin resistance or insufficient pancreatic insulin production (Bunsroem et al., 2022). According to a recent study published by the International Diabetes Federation in 2022, there are currently approximately 536.6 million people with diabetes worldwide (Inayati et al., 2022), of which 95% are patients with type 2 diabetes (T2DM). Without immediate and effective interventions, the prevalence of diabetes will rise dramatically to 11.3% (642.7 million people) by 2030 and 12.2% (783.2 million people) by 2045(Inayati et al., 2022). The continued progression of the disease can

* Corresponding author. Key Laboratory of Tropical Marine Bio-resources and Ecology, Guangdong Key Laboratory of Marine Materia Medica, South China Sea Institute of Oceanology, Chinese Academy of Sciences, 164 West Xingang Road, Guangzhou, 510301, Guangdong, China.
E-mail address: jypan@scsio.ac.cn (J. Pan).

https://doi.org/10.1016/j.crfs.2023.100446
Received 14 October 2022; Received in revised form 4 January 2023; Accepted 13 January 2023
Available online 14 January 2023

lead to numerous long-term microvascular and macrovascular complications, increasing the risk of premature death (Fowler, 2011). In 2021, diabetes caused 6.7 million deaths, the equivalent of one death every 7 s. It imposes a significant economic burden on global health care systems, with at least $966 million spent on the disease annually, equivalent to 9% of global health spending (H. Sun et al., 2022). Maintaining normal blood glucose levels is the most effective treatment to prevent or delay the progression and complications of T2DM. Currently, diabetes treatments focus on hyperglycemia control mainly include oral antidiabetic drugs and insulin injections. Numerous studies have shown that α-amylase (AAM), α-glucosidase (AG) and dipeptidyl peptidase (DPP-IV) are the key enzymes in blood glucose regulation, and inhibiting the activities of these enzymes is considered to be an effective strategy to control T2DM (Ramírez Fuentes et al., 2021). Nevertheless, over the past few years, the commonly used antidiabetic drugs, such as biguanides and sulfonylureas, have not only conferred significant glycemic control effects but are also accompanied by side effects such as abdominal distension, liver injury, diarrhea, and different degrees of drug resistance (Zhou et al., 2022). Therefore, there is an urgent need to discover safer and natural alternative active ingredients without toxicity and adverse effects to tackle this disorder.

In recent years, many studies have suggested that different food protein hydrolysates and peptides derived from meat products, dairy products, plants and marine organisms are excellent sources of bioactive peptides for application against lifestyle-related metabolic diseases (Nong and Hsu, 2021). Alternative therapies based on food-derived proteins or peptides, which are increasingly recognized as potential natural active agents, have been proposed for the prevention and control of diabetes. They have been verified to be safer, milder and more easily absorbed than synthetic drugs (Harnedy and FitzGerald, 2012). In addition to terrestrial sources, marine organisms, which have attracted much research attention in recent years, are considered to be rich sources of bioactive molecules with diverse structures and various biological effects on the human body. Increasing attention has been devoted to the biological functions of protein hydrolysates and biopeptides in marine bioactive materials. Among them, hydrolysates containing bioactive peptides in fish muscle, viscera and their processing byproducts have attracted much attention because of their multifunctional activities, such as antioxidant, immunomodulatory, antidiabetic, anti-inflammatory, antibacterial, anticancer and antihypertensive effects (Phadke et al., 2021). In general, the protein level of fish meat usually ranges between 17% and 22% (w/w): this protein is easily digestible and provides all of the essential amino acids for human dietary needs. In addition, fish protein hydrolysates have excellent functional characteristics, such as high solubility, emulsification, and foaming properties, and can be used as ingredients in a variety of food formulations with minimal sociocultural or religious restrictions (Harnedy-Rothwell et al., 2021; Siddik et al., 2021). These peptides are not active when they are encrypted in the native protein sequences but exhibit beneficial health effects when they are released from the parent protein after proteolysis (Auestad and Layman, 2021). The functions they exert depend on the amino acid composition, sequence, length, hydrophobicity and charges (Chalamaiah et al., 2019). At present, some protein hydrolysates and peptides isolated and prepared from marine fish have been shown to have regulatory effects on T2DM, especially on the inhibition of molecular targets such as AG, AAM and DPP-IV. Nasri et al. used the enzyme from B. mojavensis A21 to prepare goby fish protein hydrolysates and proved that as compared with the model group, the inhibition rate of AAM was reduced by 62% by the hydrolysates (Nasri et al., 2015). Harnedy et al. and Huang et al. reported antidiabetic peptides from salmon, whiting and tuna, which showed excellent DPP-IV inhibitory activity *in vitro* (Huang et al., 2012; Harnedy et al., 2018a,b; Harnedy et al., 2018, 2018). Sarteshnizi, R. A. et al. found that fractions from sardine muscle hydrolysates treated by papain or alcalase hydrolysis had good inhibitory effects on α-glucosidase (IC_{50} = 8.68 ± 0.41 mg/mL) (Sarteshnizi et al., 2021).

However, the identification and screening of peptides with AG, AAM and DPP-IV inhibitory effects from natural protein hydrolysates are complex and time-consuming processes. What is more difficult is that the hypoglycemic mechanisms of these screened active peptides cannot be further elucidated due to the limitations of preparation quantity. For rapid and targeted screening of potentially bioactive peptide sequences from proteins, the development of bioinformatics-based approaches can effectively compensate for the expensive and time-consuming drawbacks of current routine laboratory analysis. One of the research directions involving targeted peptides is the application of *in silico* approaches, which could mimic *in vivo* situations to some extent and reveal the possible mechanisms of interactions of peptides with target enzymes. These *in silico* tools include databases (e.g., BIOPEP-UWM, PeptideDB), websites (e.g., PepDraw, PeptideRanker), and related programs (e.g., Discovery Studio, AutoDock). These tools can be used to assist in the alignment of protein and peptide sequences, the prediction of physicochemical properties and bioactivity of peptides, as well as the structure-activity relationships between receptor-peptide complexes (Xiao et al., 2022). Thus, the combination of a peptidomic approach and an *in silico* approach can be used to screen hypoglycemic peptides or their precursors by comparing and analyzing the differential peptides of different hydrolysates (C. Wang et al., 2020).

Trachinotus ovatus, also known as golden pompano, is a species of carnivorous marine fish that mainly preys on some zooplankton and small crustaceans, shellfish and fish. It is widely distributed in the temperate and subtropical waters of the Pacific Ocean, Indian Ocean and Atlantic Ocean (J.L. Sun et al., 2022) and has become an important economically farmed fish in southern China due to its rapid growth, palatability, the nutritional quality of its flesh, suitability for cage culture, increasing market demand, and considerable economic efficiency (Zhao et al., 2022). Over the past decade, the annual output of *T. ovatus* increased from 75,000 tons to 168,000 tons and was worth 40 billion yuan due to the large-scale application of inshore net pens and intensive breeding modes in China (Qin et al., 2022). However, due to the lack of high-value utilization, this output becomes low-value aquatic products in the harvest season. *T. ovatus* has a high protein content (19.3%) and a balanced amino acid composition, but there have been few reports in the literature on active peptides screened from its protein hydrolysates, e.g., XOD inhibitory peptides and umami enhancing peptides (Hou et al., 2022). There is still a knowledge gap about the hydrolysates or peptides of *T. ovatus*. In our previous study on glucose and lipid metabolism, the hypolipidemic activity of protein hydrolysates and their peptides in *T. ovatus* was reported (Wan et al., 2020). However, to the best of our knowledge, there have been no attempts to investigate its antidiabetic activity and mechanism of inhibiting related metabolic enzymes. Accordingly, the objective of the present study was to investigate the potential antidiabetic effects of protein hydrolysates obtained by enzymatic hydrolysis from the muscles of *T. ovatus* on diabetic mice induced by streptozotocin (STZ). Additionally, the active peptide sequences in the protein hydrolysates were identified and screened by HPLC-ESI-Q-TOF-MS/MS combined with bioinformatic tools, and the potential mechanisms of the peptides inhibiting AAM and DPP-IV were preliminarily analyzed by molecular docking. Therefore, this study will provide new active functional food or nutraceutical ingredients for the management of diabetes and provide a theoretical basis for the high-value comprehensive utilization of *T. ovatus*.

2. Materials and methods

2.1. Materials and chemicals

T. ovatus were purchased from the Huangsha aquatic products wholesale market in Guangzhou, China. Trypsin (>250 NFU/mg) was purchased from Solarbio Biotechnology Corp. (Beijing, China). Pancreatic α-amylase (AAM), human recombinant dipeptidyl peptidase IV (DPP-IV), starch, diprotin A(Ile-Pro-Ile), acarbose (purity ≥95.0%), Gly-

Pro-p-nitroanilide and solvents as well as reagents for chromatography were purchased from Sigma Aldrich (St. Louis, MO, USA). The creatinine (crea) kit, serum urea (urea) kit, and insulin (INS) kit were purchased from Zhongsheng Beikong Biotechnology Co., Ltd. (Beijing, China). Superoxide dismutase (SOD), catalase (CAT) and glutathione peroxidase (GPX) kits were purchased from Nanjing Jiancheng Bioengineering Institute (Nanjing, China). All other chemicals and reagents were of analytical grade.

2.2. Preparation of T. ovatus hydrolysates

The fish were cleaned with tap water, and then the muscles were separated and rinsed with cold distilled water to remove the contaminants. The fish meat of *T. ovatus* was homogenized in a blender (Joyoung, JYL-Y910) for approximately 2 min. The homogenates were then hydrolyzed for 4 h (37 °C, pH 8.0) with trypsin at an enzyme to substrate ratio of 3000 U/g. After hydrolysis, the reaction was stopped by incubation in a boiling water bath for 10 min to inactivate the enzyme, followed by centrifugation at 8000 rpm (500 mL centrifuge tube, Avanti J-26S XP Centrifuge, Beckman Coulter, Inc. 250 S. Kraemer Blvd., Brea, CA 92821, USA.) for 20 min at 4 °C. A part of the supernatant was collected, concentrated and lyophilized to obtain *T. ovatus* hydrolysates (TOH). The other supernatant was collected and fractionated by ultrafiltration cassettes (Vivaflow 200: 10k and 3k molecular weight cutoff (MWCO) PES, Sartorius Stedim Biotech GmbH Göttingen, Germany) in an ice-water bath. The ultrafiltration fractions with molecular weights of 10 kDa–3 kDa (TOH-1) and <3 kDa (TOH-2) were collected.

2.3. In vitro AAM inhibitory activity assay

The *in vitro* inhibitory effect of the hydrolysates and fractions against AAM activity was assessed according to the method of Awosika and Aluko (Awosika and Aluko, 2019) with some modifications. The lyophilized hydrolysates or fraction samples and AAM were dissolved in 20 mmol/L sodium phosphate buffer with 6.7 mmol/L NaCl (pH 6.9) to prepare 10 mg/mL and 1 U/mL solutions, respectively. Briefly, 20 μL of the samples or acarbose (positive control) and 10 μL of AAM were mixed and incubated in a shaker bath at 37 °C for 15 min. Next, 500 μL of 1% starch dissolved in the same 20 mmol/L sodium phosphate buffer was added to the reaction mixture and incubated at 37 °C for 5 min. At the end of the reaction, 600 μL of the dinitrosalicylic acid colored reagent was added to the mixture, and then the test tubes were placed in a water bath at 100 °C for 5 min to inactivate the enzyme. After the reaction mixture was cooled to room temperature, 200 μL was transferred into respective wells of a 96-well plate, and the absorbance at 540 nm was measured with a microplate reader. The enzyme inhibition was calculated according to equation (1):

$$\text{enzyme inhibition } (\%) = \frac{A_0 - A_i}{A_0} \times 100 \quad (1)$$

where A_0 is the absorbance of the control (100% activity in the absence of inhibition) and A_i is the absorbance of reaction containing acarbose or protein/peptide fractions.

2.4. In vitro DPP-IV inhibitory activity assay

The *in vitro* DPP-IV inhibitory activity test for the hydrolysates and the fractions was performed as previously described by Nongonierma and Fitzgerald (Nongonierma and FitzGerald, 2014) with slight modifications. Briefly, the hydrolysates and fractions were dispersed in Tris-HCl buffer (100 mmol/L, pH 8.0). Fifty μL of the enzyme at 0.02 U/mL mixed with 50 μL of sample was preincubated at 37 °C for 10 min, after which 50 μL of 1 mmol/L Gly-Pro-*p*-nitroanilide was added to initiate the reaction. After incubating at 37 °C for 60 min, the absorbance was measured at 405 nm by a microplate reader (Synergy LX, BioTek, USA). For the negative control, Tris-HCl buffer was used as a negative control instead of the samples. Diprotin A was used as the positive control, and DPP-IV inhibition was calculated by equation (2):

$$\text{enzyme inhibition } (\%) = \left(1 - \frac{A_s - A_{sc}}{A_n - A_{nc}}\right) \times 100 \quad (2)$$

where A_s represents the absorbance of the reaction mixture containing all of the reactants; A_{sc} represents the absorbance of the sample background; A_n represents the absorbance without sample or diprotin A; and A_{nc} represents the absorbance of the mixture without sample and DPP-IV.

2.5. Purification of AAM and DPP-IV inhibitory peptides

2.5.1. Separation by gel filtration chromatography

The ultrafiltration fractions of the protein hydrolysates of *T. ovatus* were evaluated by AAM and DPP-IV inhibitory activities, and the most potent fraction (TOH-2) was selected for subsequent purification. The freeze-dried ultrafiltration fractions were dispersed in water at a concentration of 100 mg/mL, passed through 0.22 μm filters and analyzed with a QuikSep-50IID HPLC system (H&E Technology) on a Sephadex G-15 column (3.0 × 45 cm). The mixture was eluted with distilled water at a flow rate of 10 mL/min and monitored at 220 nm and 280 nm. The obtained fractions were lyophilized for further determination of AAM and DPP-IV inhibitory activities.

2.5.2. Purification by reversed-phase high-performance liquid chromatography (RP-HPLC)

The fractions (F4 and F6) separated by gel filtration chromatography with better AAM and DPP-IV inhibition effects were further purified through RP-HPLC with an Agilent 1260 HPLC (USA) on a YMC-Pack ODS-A column (250 × 4.6 mm I.D. S-5 μm, 12 nm) at 40 °C. The freeze-dried samples were dispersed in ultrapure water (20 mg/mL), and 20 μL of solution was injected into a C18 column after passing through a 0.22 μm filter. The mobile phase consisted of 0.1% formic acid in water (solvent A) and 0.1% formic acid in methanol (solvent B). A linear gradient elution program was performed as follows: for F4, 0–10 min 6% B, 10–45 min 50% B, 45–47 min 60% B, 47–50 min 90% B, 50–53 min 90% B, 53–55 min 4% B; for F6, 0–10 min 6% B, 10–25 min 50% B, 25–27 min 60% B, 27–30 min 90% B, 30–33 min 90% B, 33–35 min 4% B. Gradient elution was performed at a flow rate of 1.0 mL/min, and a 5 mL fraction was accordingly collected in each tube. The eluted peaks were monitored by absorbance at 220 nm using a UV/visible detector.

2.6. Identification of amino acid sequences by LC-ESI-Q-TOF-MS/MS and in silico analysis

The fractions derived from RP-HPLC purification were collected and subjected to LC-ESI-Q-TOF-MS/MS analysis on a Bruker QTOF Premier mass spectrometer (Bruker Da; TPMOCS Inc., Billerica, MA) equipped with an electrospray ion source and coupled with an HPLC system (Agilent 1260, USA). Samples of 5 μL treated with a 0.22 μm filter were loaded onto a YMC-Pack ODS-AQ column (250 × 4.6 mm, 5 μm) at 40 °C, and components were eluted with a flow rate of 0.3 mL/min of water–0.1% formic acid (buffer A) and methanol-0.1% formic acid (buffer B). The gradient elution procedure was consistent with the method mentioned above. The MS spectra were acquired under the positive ion mode at a capillary voltage of 4.5 kV with full scans ranging from 200 to 2000 m/z. The other mass spectrometric parameters were set as follows: nebulizer gas, nitrogen, 0.8 bar; dry gas, nitrogen, 5.0 L/min, 180 °C; endplate offset, 500 V; quadrupole ion energy, 5 eV; collision-induced dissociation energy, 10 eV. All data acquisition and analysis were performed using PEAKS Studio 6.0 software (Bioinformatics Solutions Inc., Waterloo, Canada).

The identified peptides were then screened by the PeptideRanker

web server available at http://distilldeep.ucd.ie/PeptideRanker/ (accessed on 6 July 2022). A PeptideRanker score close to 1 (in the 0–1 range) indicates that the amino acid sequence exhibits a high probability of bioactivity. Therefore, those identified peptides with a score greater than 0.8 were designated as potentially bioactive peptides and subjected to potential biological activity assessment using BIOPEP-UWM available at http://www.uwm.edu.pl/biochemia/index.php/en/biopep (accessed on 13 July 2022). The physicochemical properties of the screened active peptides were evaluated using *in silico* tools. The hydrophobicity, net charge, PI (isoelectric point) value, and water solubility were analyzed using PepDraw (http://pepdraw.com/) and PepCalc (https://pepcalc.com/) (Zhao et al., 2020).

2.7. Preliminary molecular binding mechanism of screened peptides against AAM and DPP-IV enzymes

In silico molecular docking of these peptides and enzymes was conducted based on the programs of the web server Pepsite2 (http://pepsite2.russelllab.org/, accessed on 22–28 July 2022) and Discovery Studio platform (DS, version 4.5) to determine how the identified peptides bind to the targeted enzymes (AAM and DPP-IV) to exert their effects (Mudgil et al., 2020). Peptides and enzymes were selected as ligands and receptors, respectively. The crystal structures of AAM (PDB code: 3BAJ, 2.10 Å) and DPP-IV (PDB code: 4A5S, 1.62 Å) were derived from the RCSB PDB database (https://www.rcsb.org/). The two-dimensional (2D) and three-dimensional (3D) structures of the peptides were constructed by the ChemDraw Ultra 20.0 package (CambridgeSoft, Waltham, MA, USA). Before docking, water molecules and ligands as well as excess proteins were removed from the crystal structure of the receptor, and polar hydrogen atoms were added. The selection of the best interacting peptides and protein receptors was performed based on the statistical significance output, and only $p < 0.05$ was considered significant. In addition, the hotspots of enzymes bound by peptides were also considered. Ten ligand docking configurations were generated, and the best docking poses of the peptides in the active sites of receptors were obtained according to the p values and were illustrated by ligplot^{+}(version v.2.2.5). Furthermore, docking confirmation, including the 3D crystal structure and catalytic site interactions, was visualized by DS based on the minimum binding energy (kcal/mol).

2.8. In vivo experiment

2.8.1. Animals and treatments

Male Kunming (KM) mice, weighing 18–22 g, were obtained from Guangdong Medical Laboratory Animal Center (Foshan, China, certification no. SCXK 2016–0029) and were housed in a storage room. Animals were kept in stainless steel cages under standard laboratory conditions with a constant temperature of 25 ± 1 °C, relative humidity of 55 ± 5% and an alternating 12 h light/dark cycle. The mice were allowed free access to tap water and food during the experimental period. All animal procedures were performed in accordance with the U. S. National Institutes of Health Guide for the Care and Use of Laboratory Animals (Publication No. 85–23, revised 1996), and experimental protocols were approved by the Animal Ethics Committee of Sun Yat-sen University (license: SYXK-(Yue) 2014–0020). After one week of environmental accommodation, the mice were weighed, and their fasting blood glucose (FBG) was measured before the experiment. At the beginning of the experiment, all of the mice fasted without water for 12 h. All the animals, except the normal control group (NC, n = 10), were treated with an intraperitoneal injection of freshly prepared streptozotocin (STZ) at a dose of 150 mg/kg (STZ dissolved in 0.1 M citrate buffer, pH 4.5). The NC mice were injected with the same volume of citrate buffer. To detect the FBG level, blood samples were collected from the tails of mice after 72 h, and the mice whose FBG levels were ≥11.1 mmol/L were selected as a diabetic model. Subsequently, the diabetic mice were randomly divided into five groups (n = 50) as follows: the DC group (DC, diabetic control mice, n = 10), the low-dose TOH group (TOH-L, 100 mg/kg body weight, n = 10), the medium-dose TOH group (TOH-M, 500 mg/kg body weight, n = 10), the high-dose TOH group (TOH-H, 1000 mg/kg body weight, n = 10) and the Met group (Met, with metformin treatment used as the positive control, 250 mg/kg body weight, n = 10). TOH and Met were dissolved in normal saline and administered daily by oral gavage at a dose of 0.2 mL/mouse. Correspondingly, the NC and DC groups received an equivalent volume of normal saline. All animals received oral administration for 4 weeks. The general signs and food intake of the mice were measured daily, and the blood glucose levels and body weight changes were monitored and recorded weekly.

2.8.2. Blood and tissue sample collection

At the end of the experimental period (12 h overnight fast), the mice were deeply anesthetized with ether and euthanasia via decapitation to avoid any additional stress, and the blood samples were collected in heparin tubes. Plasma samples were separated and collected after centrifugation (4000 rpm, 15 min, 4 °C) and frozen in liquid nitrogen at −80 °C prior to the biochemical analysis. Samples of pancreas, liver and kidney were excised from the experimental mice, rinsed with cold 0.9% phosphate buffered saline, wiped with filter paper and weighed. The relative organ weight was calculated and defined as the weight of the organ (g)/body weight (g).

2.8.3. Biochemical analysis

The levels of blood glucose, crea and urea were measured by a FAITH-1000 automatic biochemical analyzer (Nanjing Laura Electronics Co., Ltd, Nanjing, China). The serum insulin concentration was determined by an enzyme-linked immunosorbent assay (ELISA). An ultrasensitive mouse insulin ELISA kit (Thermo Fisher Scientific, Thermo Electron Co., Waltham, MA, USA) coupled with a Wellscan MK3 microplate reader (Leibo Co., Finland) was used for the measurement. The levels of SOD, CAT, and GPX were assayed enzymatically using commercial kits according to the manufacturer's instructions (Jiancheng Bioengineering Institute, Nanjing, China).

2.8.4. Histopathological examination

At the end of the experiment, the kidneys and pancreas of the mice were removed, fixed in 10% neutral formaldehyde, and routinely dehydrated and embedded in paraffin. Paraffin sections of kidney tissues (4 μm thick) were stained with conventional HE staining and Masson staining. Pancreatic tissue sections were subjected to stained with HE staining and elastic fiber staining. The histopathological changes in the kidney and pancreas were observed under an Olympus light microscope (CX31; Olympus, Japan).

2.9. Statistical analysis

All analytical data were expressed as the mean ± standard deviation and analyzed using SPSS 24.0 software (IBM Inc., New York, USA). All assays were tested in 3 replicates. One-way analysis of variance (ANOVA) with Tukey's post hoc test was used to compare significant differences. The results were considered to be statistically significant at $p < 0.05$.

3. Results and discussion

3.1. Effects of TOH on weight change and food intake in STZ-induced diabetic mice

Diabetes mellitus is caused by insulin-dependent abnormal glucose and lipid metabolism, with typical symptoms of polydipsia, polyuria and polyphagia, and is often accompanied by chronic fatigue and sudden body weight loss (Soskolne and Klinger, 2001). Therefore, the improvement of these typical metabolic symptoms predicts the

corrective effect of drugs or active ingredients on diabetes. To investigate the effects of TOH on diabetic symptoms, physiological parameters, including body weight and food intake, were assayed in STZ-induced diabetic mice. As shown in Fig. 1A and B, at the beginning of the experiment (week 0), there was no significant difference in body weight or food intake among the treatment groups. However, as the experiment progressed, the body weight of the mice in the DC group was significantly lower than that in the NC group and the other treatment groups ($p < 0.05$), and the food intake of the mice in the DC group was significantly higher than that in the NC group and the other treatment groups ($p < 0.05$), showing typical characteristics of diabetes. However, the typical symptoms of diabetic mice were improved after the administration of TOH or Met: this was especially true for the food intake of diabetic mice, which returned to normal levels during the experimental period. However, it should be noted that in a short experimental period, similar to the effect of positive drug treatment, TOH was not able to promote the complete recovery of diabetic mice to normal body weight. Similar results were observed with other marine protein sources, such as *Palmaria palmata*, which increased body weight and reduced food intake in diabetic mice (McLaughlin et al., 2020).

3.2. Effects of TOH on random blood glucose (RBG)

Diabetes is commonly defined on the basis of fasting or postprandial blood glucose, with a random blood glucose (RBG) $\geq$ 11.1 mmol/L and/or a fasting blood glucose (FBG) $\geq$ 7 mmol/L. However, RBG is the most convenient method for population blood glucose screening, especially for the identification and diagnosis of prediabetes, and is the most commonly used test index for diabetes (Somannavar et al., 2008). The change in blood glucose is a direct reflection of the process of diabetes. As shown in Table 1, before the establishment of the diabetic mouse model, the blood glucose levels of mice in each group were maintained at the normal level. After 72 h of establishment of the diabetic mouse model, the blood glucose of the DC group increased from 5.49 $\pm$ 0.81 mmol/L before the establishment of the model to 16.23 $\pm$ 2.13 mmol/L. The blood glucose of the Met or TOH administration groups was close to that of the model group ($p > 0.05$) at the beginning of the experiment.

Table 1
Effects of TOH or Met on random blood glucose (RBG) (mmol/L) in STZ-induced diabetic mice.

group	0 week	72 h	1st week	2nd week	3rd week	4th week
DC	5.49 $\pm$ 0.81	16.23 $\pm$ 2.13	16.54 $\pm$ 2.95	18.29 $\pm$ 5.58	23.75 $\pm$ 3.90	28.39 $\pm$ 4.81
NC	5.14 $\pm$ 0.67	5.66 $\pm$ 0.47^{a}	5.55 $\pm$ 0.63^{a}	5.39 $\pm$ 0.64^{a}	5.28 $\pm$ 0.95^{a}	5.43 $\pm$ 0.69^{a}
Met	5.34 $\pm$ 0.85	15.34 $\pm$ 1.82^{b}	12.00 $\pm$ 4.40^{b}	9.63 $\pm$ 2.39^{a}	14.34 $\pm$ 3.36^{ab}	15.53 $\pm$ 4.11^{ab}
TOH-L	5.39 $\pm$ 0.44	16.10 $\pm$ 1.23^{b}	14.95 $\pm$ 3.99^{b}	14.68 $\pm$ 2.48^{bc}	18.86 $\pm$ 2.07^{ab}	24.09 $\pm$ 5.68^{bc}
TOH-M	5.49 $\pm$ 0.74	15.30 $\pm$ 2.31^{b}	15.01 $\pm$ 2.77^{b}	12.78 $\pm$ 3.25^{ab}	18.73 $\pm$ 3.61^{ab}	22.74 $\pm$ 3.78^{abc}
TOH-H	5.54 $\pm$ 0.58	14.75 $\pm$ 2.12^{b}	13.63 $\pm$ 3.49^{b}	13.00 $\pm$ 3.34^{ab}	17.73 $\pm$ 3.75^{ab}	19.99 $\pm$ 2.68^{ab}

Data are expressed as the mean $\pm$ SD (n = 10). The lowercase letter a indicates $p < 0.05$ vs. mice in the DC group, the lowercase letter b indicates $p < 0.05$ vs. mice in the NC group, and the lowercase letter c indicates $p < 0.05$ vs. mice in the Met group. DC: diabetic control; NC: normal control; Met: metformin for the positive control (250 mg/kg); TOH-L: low-dose *T. ovatus* hydrolysates (100 mg/kg); TOH-M: medium-dose *T. ovatus* hydrolysates (500 mg/kg); TOH-H: high-dose *T. ovatus* hydrolysates (1000 mg/kg).

After 1 week of administration, there was a slight decrease in RBG in the TOH and Met groups ($p > 0.05$), but the RBG level remained higher than that of the NC group ($p < 0.05$). After 2 weeks of administration, the RBG of the Met group was close to that of the NC group ($p > 0.05$). There was no significant difference in RBG levels between the TOH-M and TOH-H groups and the Met group ($p > 0.05$), but the RBG level remained significantly higher than that of the NC group. As the experiment progressed, the blood glucose of the DC group continued to increase. At the 3rd and 4th weeks of administration, the blood glucose level of each treated group could be significantly decreased but could not return to the normal blood glucose level ($p < 0.05$). The hypoglycemic effect of the TOH administration groups showed a dose-dependent effect, and there was no statistically significant difference in the hypoglycemic effect between the TOH-H group and the Met group ($p > 0.05$), which

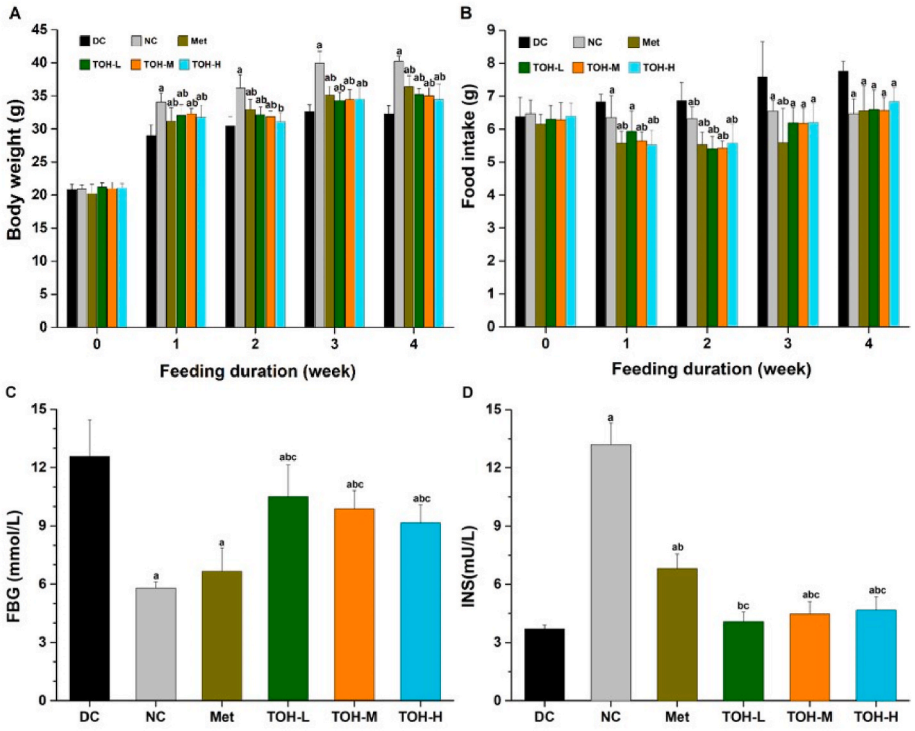

Fig. 1. Effects of TOH and Met on (A) weight change, (B) food intake, (C) fasting blood glucose (FBG) and (D) serum insulin (INS) in STZ-induced diabetic mice over four weeks. Values are expressed as the mean $\pm$ SD (n = 10). The lowercase letter a indicates $p < 0.05$ vs. mice in the DC group, the lowercase letter b indicates $p < 0.05$ vs. mice in the NC group, and the lowercase letter c indicates $p < 0.05$ vs. mice in the Met group. DC: diabetic control; NC: normal control; Met: metformin for the positive control (250 mg/kg); TOH-L: low-dose *T. ovatus* hydrolysates (100 mg/kg); TOH-M: medium-dose *T. ovatus* hydrolysates (500 mg/kg); TOH-H: high-dose *T. ovatus* hydrolysates (1000 mg/kg).

proved the effect of TOH in improving RBG in diabetic mice and indirectly indicated that STZ destroyed blood glucose regulation homeostasis in mice.

3.3. Effects of TOH on fasting blood glucose (FBG) and serum insulin (INS)

It has been documented that intake of protein hydrolysates can effectively enhance the postprandial insulin response and reduce postprandial blood glucose levels (Jonker et al., 2011). To investigate the effect of TOH intake on the regulation of glucose metabolism and insulin action, we assayed the fasting blood glucose (FBG) and serum insulin (INS) levels. As illustrated in Fig. 1C, compared with the NC group (5.79 ± 0.33 mmol/L), a sharp increase (by 117%, $p < 0.05$) in FBG was observed in mice from the DC group (12.58 ± 1.87 mmol/L), while the TOH groups showed a significant dose-dependent decline in the glucose level (decreases of 16%, 21% and 27%, respectively, $p < 0.05$) compared with the DC group. The positive control drug metformin had the most obvious hypoglycemic effect. Compared with the DC group, the FBG of the Met group was reduced by 47%, and there was no significant difference compared with the NC group ($p > 0.05$). Although the TOH group did not restore blood glucose to normal levels in diabetic mice as did the Met group ($p < 0.05$), the hypoglycemic efficiency of the TOH-H group reached 58% of that of metformin, indicating its considerable effect. To determine whether the decrease in blood glucose was attributable to improved insulin secretion, serum insulin levels were measured and compared between the DC group and the TOH or Met intervention group. A remarkable decrease in the INS level (Fig. 1D) was observed in the DC group, whereas the INS level notably increased ($p < 0.05$) in the corresponding groups after TOH-M/TOH-H or Met intervention compared with that in the DC group.

The results showed that long-term administration of TOH could effectively improve insulin secretion in diabetic mice. Several previous intervention studies have reported improvements in insulin sensitivity and glucose tolerance after fish protein supplementation in humans and rodents (Jensen et al., 2019). In contrast to those studies, TOH did not improve glucose homeostasis by improving insulin resistance, which was manifested in the significant decrease in insulin levels in DM mice in our study, rather than the compensatory insulin secretion caused by glucose rise, as shown in other studies. This is mainly attributed to the loss of pancreatic β-cells induced by STZ and their functional defects, which lead to decreased postprandial insulin secretion and hyperglycemia, rather than the result of insulin resistance. Similar to our results, several other studies have shown that rice gluten, an alkali-soluble protein, inhibits postprandial glucose elevation by promoting insulin secretion (Ishikawa et al., 2015). This may be attributed to the inhibitory effects of some protein hydrolysates on DPP-IV. It has been found that long-term (4–7 weeks) treatment of STZ-induced diabetic rats with the DPP-IV inhibitors sitagliptin and isoleucine thiazolidine can reduce blood glucose levels and increase pancreatic insulin content and the number of small islets (Deacon and Holst, 2006). This is consistent with our study on the DPP-IV inhibition effect of TOH (Section 3.6). These data collectively indicate that TOH administration, especially at a high dose, could effectively enhance insulin secretion and improve blood glucose levels.

3.4. Effects of TOH on liver and kidney markers

The liver is the vital organ for the metabolism, detoxification, storage and excretion of xenobiotics and their metabolites, particularly serving as the center of glucose metabolism. The kidney plays a distinctive role in glucose homeostasis. It promotes glucose homeostasis through processes such as gluconeogenesis, glucose filtration, glucose reabsorption and glucose consumption. The liver and kidney are the two major organs that bear the brunt of elevated hyperglycemia. Elevated levels of serum biomarkers of liver and kidney injury have been widely reported in diabetic models (Arunachalam and Parimelazhagan, 2013). Current studies generally consider oxidative stress to play a primary role in the onset and development of diabetes. Most of the defense mechanisms against reactive oxygen species (ROS) are related to the activities of antioxidant enzymes that remove excess ROS, especially the antioxidant enzymes SOD, CAT and GPX in the liver (Gao et al., 2021). As shown in Fig. 2 (A-C), compared with the NC group, the activities of SOD, CAT and GPX in the DC group notably decreased ($p < 0.05$). Nevertheless, oral administration of TOH yielded a remarkable elevation of SOD, CAT and GPX levels. The results indicated that TOH could antagonize the side effects of ROS and oxidative stress in organs and tissues.

Given that many kidney cell types are insulin sensitive, high blood glucose levels can lead to severe renal tissue damage and kidney dysfunction. Serum creatinine and urea levels are considered to be prognostic indicators of renal function (Shady et al., 2022). As shown in Fig. 2E and F, abnormal increases in crea and urea levels in the serum were observed in the DC group ($p < 0.05$), indicating renal dysfunction. After metformin intervention, crea and urea decreased significantly compared with the DC group ($p < 0.05$). However, although the TOH group exhibited a significantly reduced urea level ($p < 0.05$), the crea level was not improved ($p > 0.05$). To validate these serological findings, liver and kidney indices were measured. As shown in Fig. 2D, compared with the NC group, the liver and kidney indices of mice in the DC group were significantly increased, suggesting that the liver and kidney of diabetic mice developed edema after STZ injection. After TOH administration, the liver and kidney indices of diabetic mice were significantly decreased ($p < 0.05$), and edema symptoms were significantly relieved. These results indicated that TOH can ameliorate liver and kidney injury in STZ-induced diabetic mice.

3.5. Histopathological observations

Since many renal cell types are insulin sensitive, chronically high blood glucose levels can lead to severe renal dysfunction, which in turn affects glucose metabolism. In parallel, damage to pancreatic tissue also induces insulin resistance or secretion defects in diabetic mice. To evaluate whether TOH had the capacity to protect the kidney and pancreas in diabetic mice, histological determination was performed in these tissues. As illustrated in Fig. 3 (1)-B, compared with the NC group (Fig. 3 (1)-A), the DC group revealed a certain degree of renal interstitial inflammatory cell infiltration and vacuolar degeneration of renal tubular epithelial cells. After TOH or Met intervention, renal tissue morphology was relieved (Fig. 3 (1)-C-F). In addition, as observed by Masson's trichrome staining in Fig. 3 (2), there was no significant renal fibrous change in each group, which may be related to the dose of STZ and the experimental period. As shown in Fig. 4 (1)-A-B, compared with the NC group, the mice in the diabetes model group showed pathological changes of pancreatic acinar expansion, decreased islet number, and smaller islet volume. After TOH or Met intervention, the pathological changes were improved, mainly manifested in the improvement of islet regular contour morphology and the recovery of islet cell number. However, the islet volume and islet number were still lower than those of the control group (Fig. 4 (1)-C-F). On the other hand, there was no significant pancreatic fibrosis in any group. With TOH intervention, islet volume and cell number showed dose-dependent improvement (Fig. 4 (2)). Similar results have been reported previously in that oligopeptides from marine salmon skin, silk protein hydrolysates and *Momordica charantia* peptides showed high antidiabetic activity by protecting kidney tissue and pancreatic *β*-cells (Liao et al., 2022).

3.6. Bioassay-guided fractionation of peptides from the T. ovatus protein hydrolysates

The carbohydrates digestive enzymes α-glucosidase (AG) and α-amylase (AAM) are critically involved in carbohydrates digestion into absorbable monosaccharides. Therefore, the inhibitors of both AAM,

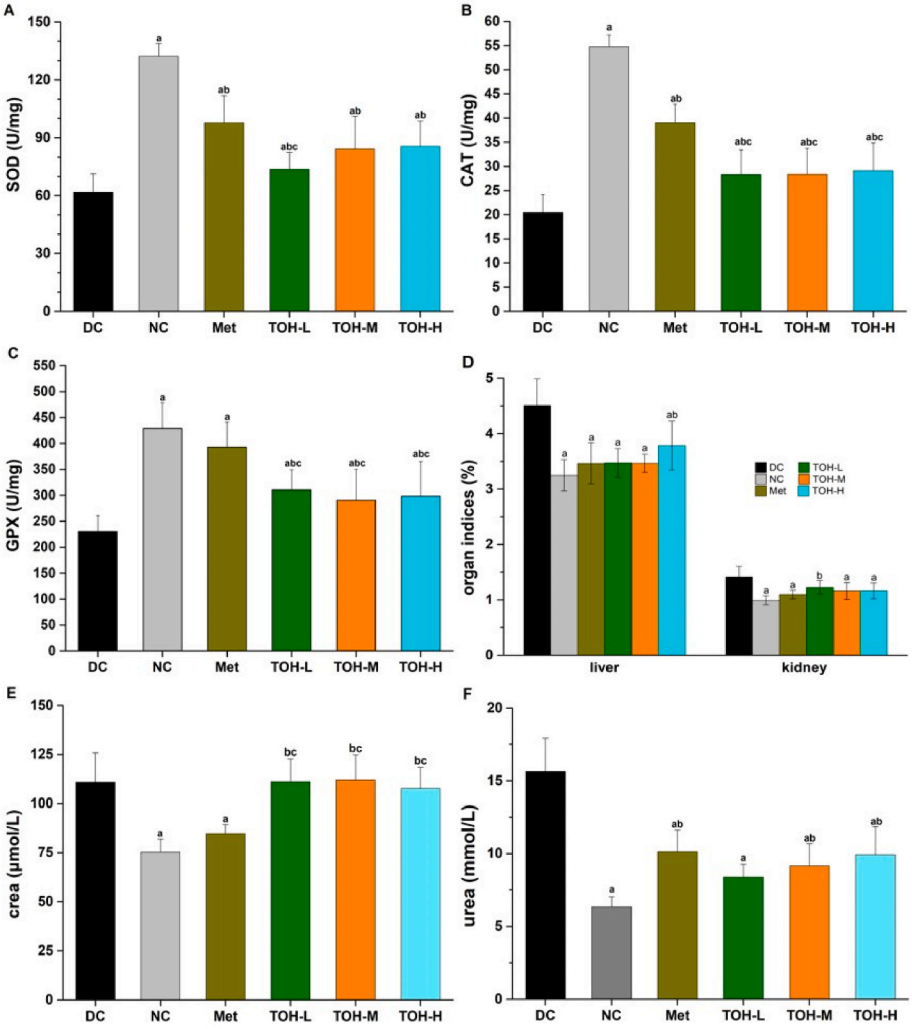

Fig. 2. Effects of TOH and Met on liver and kidney markers in STZ-induced diabetic mice. (A) Liver SOD level; (B) Liver CAT level; (C) Liver GPX level; (D) organ indices for liver and kidney (organ index was defined as the weight of the organ (g)/body weight (g)); (E) serum creatinine level and (F) serum urea level. Data are expressed as the mean ± SD (n = 10). The lowercase letter a indicates $p < 0.05$ vs. mice in the DC group, the lowercase letter b indicates $p < 0.05$ vs. mice in the NC group, and the lowercase letter c indicates $p < 0.05$ vs. mice in the Met group. DC: diabetic control; NC: normal control; Met: metformin for the positive control (250 mg/kg); TOH-L: low-dose *T. ovatus* hydrolysates (100 mg/kg); TOH-M: medium-dose *T. ovatus* hydrolysates (500 mg/kg); TOH-H: high-dose *T. ovatus* hydrolysates (1000 mg/kg).

which mainly breaks down long-chain carbohydrates (e.g., starch), and AG, which is primarily responsible for catalyzing the cleavage of glucose from disaccharides, effectively retard glucose uptake. In addition, dipeptidyl peptidase-IV (DPP-IV) mainly degrades incretin hormones, including glucagon-like peptide-1 (GLP-1) and glucose-dependent insulinotropic polypeptide (GIP), which promote postprandial insulin secretion. Therefore, inhibition of DPP-IV can effectively prevent incretin degradation and improve glycemic regulation (Yu et al., 2012). As shown in Fig. 5A, the protein hydrolysates of *T. ovatus* expressed a certain degree of AAM and DPP-IV inhibitory activities at the experimental concentrations. After ultrafiltration processing, TOH-2 (<3 kDa) with a smaller molecular weight showed stronger inhibitory activity. Therefore, TOH-2 was further separated by gel chromatography to obtain seven graded fractions (Fig. 5B). As shown in Fig. 5C and D, among the seven fractions, F4 and F6 exhibited stronger AAM and DPP-IV inhibitory activities, respectively, and will be subject to further structural identification. Some previous studies have reported that peptides with small molecular weights and high hydrophobicity are prone to have stronger AAM and DPP-IV inhibitory activities, especially peptides containing fewer than ten amino acids (Boachie et al., 2019). Our results are broadly similar to those described above.

3.7. Identification of bioactive peptides in a selected TOH-2 by HPLC-ESI-Q-TOF-MS/MS

The peptide sequences of the aforementioned F4 and F6 from TOH-2 selected through bioassay were further identified by HPLC-ESI-Q-TOF-MS/MS. The results revealed that 333 and 23 peptides with lengths between 2 and 14 amino acid residues were derived from F4 and F6, respectively (supplementary data-Tables S1 and S2). The peptides with potential biological activities according to comprehensive evaluation by the −10lgP value of the database, the average local confidence (ALC) value ≥ 70% and peptide rank score ≥0.80 are shown in Tables S3–S4 (supplementary data). Ultimately, a total of 37 and 4 peptides from F4 and F6, respectively, were identified as potentially active peptides. The physicochemical properties of the selected peptides showed that most of them had strong hydrophobicity and potential DPP-4 inhibitory activity.

3.8. Molecular interaction of potential T. ovatus-derived bioactive peptides with AAM and DPP- IV

The enzyme α-amylase (AAM) is known to contain three domains (A, B and C) and a catalytic triad in the A domain (Asp^{197}, Glu^{233}, Asp^{300}), where the A and C domains are the key catalytic sites and the B domain is responsible for binding to the substrate. Seventeen residues (i.e., Trp^{58}, Trp^{59}, Tyr^{62}, Tyr^{258}, His^{101}, His^{299}, His^{305}, Asp^{165}, Asp^{197}, Asp^{236}, Asp^{300}, Arg^{61}, Lys^{200}, Glu^{233}, Ile^{235}, Pro^{163} and Ala^{307}) of AAM have been reported to be involved in the binding of substrate analogs, among which residues Asp^{197} and Asp^{300} play important roles in AAM-catalyzed reactions. In addition, some studies have reported that the allosteric sites (Asp^{96}, Arg^{195}, His^{15}, Gln^{41}, Val^{42}, Ser^{43}, Pro^{44}, Arg^{337}) of AAM are prone to be occupied by active peptides, which reduces its

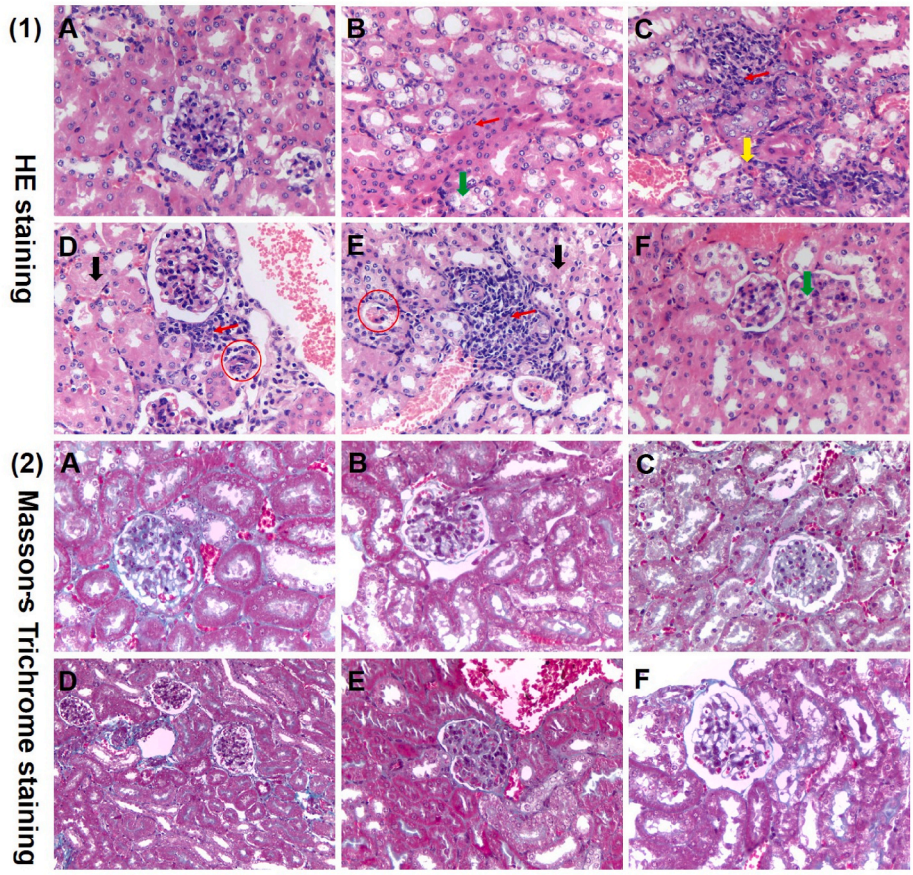

Fig. 3. Effects of TOH on the histological changes in kidney tissues in STZ-induced diabetic mice. (1) Histopathological micrograph of the kidney in normal and STZ-induced diabetic mice with H&E staining (magnification, 400 ×); (2) histopathological micrograph of the kidney in normal and STZ-induced diabetic mice by Masson's trichrome staining (magnification, 400 ×). (A)–(F) represent the NC group, DC group, Met group, TOH-L group, TOH-M group and TOH-H group, respectively. The red arrows represent inflammatory cell infiltration in the renal interstitium. The green arrowheads represent vacuolar degeneration of renal tubular epithelial cells. The yellow arrowheads represent renal interstitial hemorrhage. The black arrowheads represent interstitial fibrosis. The red circles represent glomerular atrophy. (For interpretation of the references to color in this figure legend, the reader is referred to the Web version of this article.)

activity and affects its kinetics. This indicates that the main interactions between the inhibitory peptide and AAM are electrostatic, followed by hydrophobic and hydrogen bridges, which induce its conformational change and inhibit its activity (Ngoh and Gan, 2018; Mudgil et al., 2021). DPP- IV contains a cavernous active site, which inhibitors typically compete to occupy by binding to subsites located in the cavities. The hydrophobic S1 site consists of the catalytic triad Ser^{630}--Asp^{708}/Asn^{710}-His^{740} and hydrophobic residues (Tyr^{547}, Tyr^{631}, Trp^{659}, Tyr^{662}, Tyr^{666}, Val^{711} and Val^{656}). The charged S2 sites include Glu^{205}, Glu^{206} and Arg^{125}. In addition, DPP- IV has a large cavity surrounded by Val^{207}, Ser^{209}, Arg^{358}, and Phe^{357}, known as Subsite S2' (Ritian et al., 2021).

As shown in Table 2, the screened peptides were capable of binding 4–10 hotspots of AAM, demonstrating their potential as AAM inhibitors. Among them, the five peptides FGNWR, CPPSPR, FNFSR, WPDAR, and LSGFPR from F4 and the peptide CPPTPR from F6 bind to 9–10 hotspots (Trp^{58}, Trp^{59}, Tyr^{62}, Asp^{96}, Arg^{195}, Asp^{197}, Glu^{233}, His^{299}, Asp^{300}, His^{305} and/ or His^{15}) of AAM. As mentioned above, all of these peptide sequences can bind to the three domains of AAM, especially Asp^{300} and His^{305} sites, which restrict the formation of AAM-specific conformations and structural modifications after AAM sites are occupied, reducing AAM activity. Our study also showed that most active peptides contain N, F and P amino acid residues, and almost all peptide sequences contain R residues in the C-terminus except MFK and FFK, which contain K residues in the C-terminus. This feature of AAM inhibitory peptides has been found in relevant studies. For instance, the new pentapeptide LPPLR from walnut protein hydrolysates, the tetrapeptide YSFR obtained from Chinese giant Salamander (*Andrias davidianus*) protein hydrolysate and the tripeptide GSR obtained from silkworm chrysalis showed significant AAM inhibitory activity (J. Wang et al., 2020), which was consistent with our study. In addition, smaller molecular weight peptides have stronger AAM inhibitory potential, which has been reported by many studies (Ngoh and Gan, 2016; Ngoh et al., 2016). The same result appeared in our study; that is, the screened active peptides were mainly small molecular peptides composed of 2–6 amino acids.

The interactions of the selected peptides from F4 and F6 with DPP-IV are illustrated in Table 3. The selected peptide sequences were able to bind 1–8 hotspots of DPP- IV (i.e., His^{740}, Trp^{629}, Phe^{357}, Tyr^{547}, Ser^{630}, Tyr^{631}, Trp^{659}, Tyr^{662}, Tyr^{666} and Glu^{206}). Normally, peptide fractions of less than 10 amino acids show better DPP-IV inhibitory activity. The penultimate N-terminus P residue or the C-terminus containing a P residue, often flanked by an L, V, F, A, G, or W residue, is generally considered to indicate potent DPP- IV inhibitory activity (Lacroix and Li-Chan, 2016; Boachie et al., 2019). The length of DPP- IV inhibitory peptides screened in our study was less than 10 amino acids, and several peptides with the most DPP-IV binding sites (e.g., SFGPR, NPPFK, CPPSPR and LSGFPR) all contained P residues, which was in line with the results reported above.

In particular, the hydrophobicity exerted an important effect on the AAM and DPP- IV inhibitory activities of the active peptides, as these hydrophobic amino acids may facilitate the interaction of peptides with the enzyme active sites (Nongonierma and FitzGerald, 2019). Among the 19 active peptides from F4, 13 peptides had hydrophobicity ≥50% (accounting for 58%), while 2 peptides had hydrophobicity ≥50% (accounting for 67%) among the 3 active peptides from F6 (Tables S3–S4). To show the binding effect of the active peptides with AAM and DPP- IV more visually, the pentapeptide FNFSR was used as an example, and the molecular docking results were displayed by Discovery Studio software. The docking interactions of peptide FNFSR with AAM and DPP-IV are shown in Fig. 6. The interactions between the peptide and AAM or DPP-IV mainly include nonbonding interactions, such as hydrogen bonds, van der Waals forces and π-π interactions. In addition, due to the differences in algorithms between different processing software, the potential binding sites of AAM or DPP- IV for peptides are sometimes

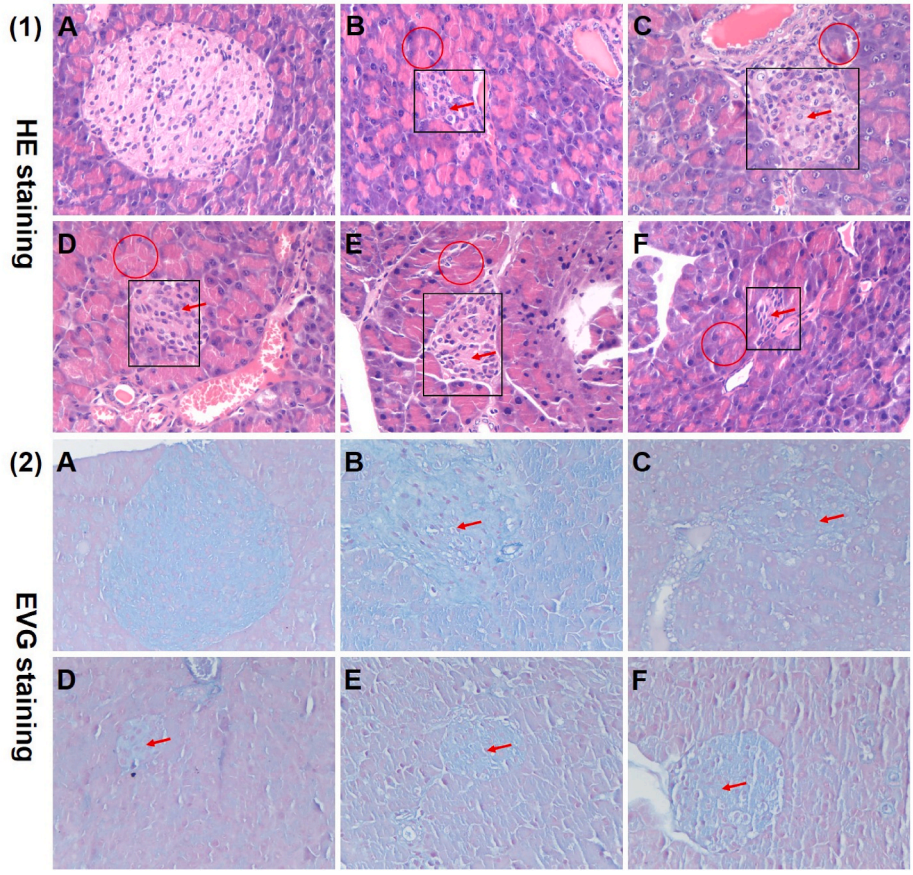

Fig. 4. Effects of TOH on the histological changes in pancreatic tissues in STZ-induced diabetic mice. (1) Histopathological micrograph of the pancreas in normal and STZ-induced diabetic mice with H&E staining (magnification, 400 ×); (2) histopathological micrograph of the pancreas in normal and STZ-induced diabetic mice with Elastic van Gieson (EVG) staining (magnification, 400 ×). (A)–(F) represent the NC group, DC group, Met group, TOH-L group, TOH-M group and TOH-H group, respectively. The red arrows represent decreased islet volume and islet number. The red circles represent necrosis or swelling of pancreatic acini. The black boxes represent the cytoplasmic degenerative changes in the center of islets of mice in the diabetic model group. (For interpretation of the references to color in this figure legend, the reader is referred to the Web version of this article.)

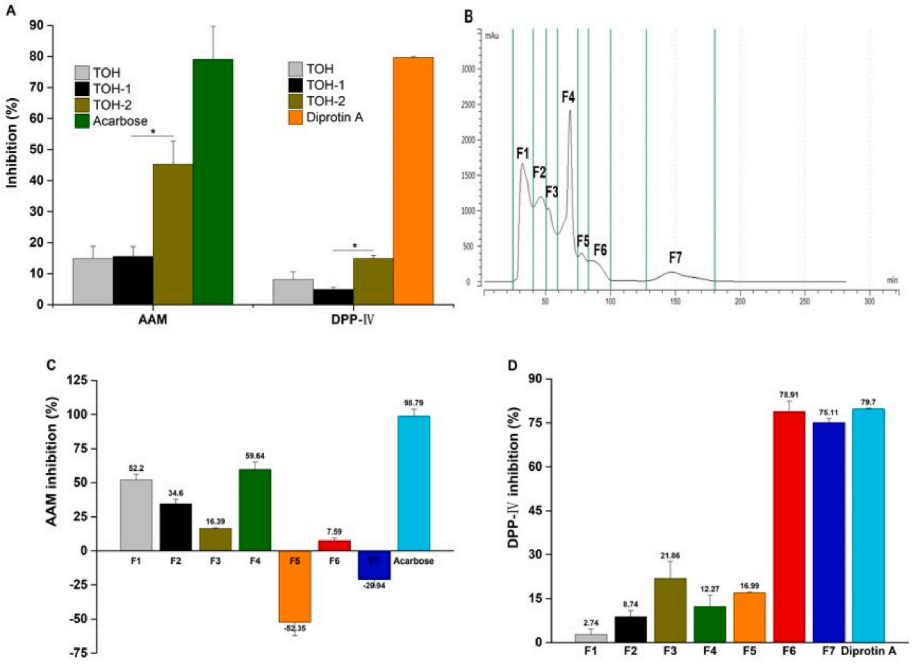

Fig. 5. Isolation and purification of TOH and its inhibitory effects on AAM and DPP-IV. (A) AAM and DPP-IV inhibitory effects of TOH and ultrafiltrations of TOH-1 and TOH-2, where $*p < 0.05$ represents the comparison between TOH-2 and TOH-1; (B) gel filtration chromatographic separation of TOH-2; (C) the inhibitory effects of the fractions isolated from TOH-2 against AAM and (D) the inhibitory effects of the fractions isolated from TOH-2 against DPP- IV. The concentrations of TOH, TOH-1 and TOH-2 as well as the fractions were 10 mg/mL. The concentrations of the positive controls of acarbose and diprotin A were 5 mg/mL and 1.2 mg/mL, respectively.

different to some extent, but this does not affect the prediction of the potential biological activities of active peptides.

4. Conclusions

This is the first time that the antidiabetic effects of protein hydrolysates and their derived peptides of *T. ovatus* have been revealed. The fish protein hydrolysates can significantly improve the typical symptoms

Table 2
Bioactive peptide sequences and their interactions with potential AAM binding sites.

Peptide sequence	Mw	Pepsite 2 (*p* value) [a]	Binding residues in peptide	Bound residues of AAM
F4				
FR	322.19	0.02352	F1, R2	Trp^{58b}, Trp^{59b}, Tyr^{62b}, His^{305b}
WR	361.20	0.009739	W1, R2	Trp^{58b}, Trp^{59b}, Tyr^{62b}, Asp^{96b}, Val^{98}, Arg^{195b}, Asp^{197b}, His^{299b}
FGNWR	679.33	0.01081	F1, G2, W4, R5	Trp^{58b}, Trp^{59b}, Tyr^{62b}, Asp^{96b}, Val^{98}, Arg^{195b}, Asp^{197b}, Glu^{233b}, Phe^{256}, Asn^{298}, His^{299b}, Asp^{300b}, His^{305b}
MFK	425.22	0.04315	M1, F2, K3	Trp^{58b}, Trp^{59b}, Tyr^{62b}, Gln^{63}, Leu^{165}, Asp^{300b}, His^{305b}
SFGPR	562.29	0.01303	F2, G3, P4, R5	Trp^{58b}, Trp^{59b}, Tyr^{62b}, Asp^{300b}, His^{305b}
NPPFK	601.32	0.0007632	N1 , P2 , P3 , F4	Trp^{58b} , Trp^{59b} , Tyr^{62b} , Asp^{300b} , His^{305b}
CPPSPR	655.31	0.0003703	C1, P2, P3, P5, R6	His^{15b}, Phe^{17}, Pro^{54}, Trp^{58b}, Trp^{59b}, Tyr^{62b}, Asp^{96b}, Arg^{195b}, His^{299b}, Asp^{300b}, His^{305b}, Asp^{356}, Trp^{357}
DFR	436.21	0.0441	D1, F2, R3	Trp^{58b}, Trp^{59b}, Tyr^{62b}, Gln^{63}, Leu^{165}, Asp^{300b}, His^{305b}
FNFSR	669.32	0.02276	F1, N2, F3, R5	His^{15b}, Phe^{17}, Trp^{58b}, Trp^{59b}, Tyr^{62b}, Asp^{96b}, Arg^{195b}, His^{299b}, Asp^{300b}, His^{305b}
LFFSR	668.36	0.04059	L1, F2, F3, R5	His^{15b}, Phe^{17}, Trp^{58b}, Trp^{59b}, Tyr^{62b}, Asp^{96b}, Arg^{195b}, His^{299b}, Asp^{300b}, His^{305b}
GFPSR	562.29	0.004154	G1, F2, P3, R5	Pro^{54}, Trp^{58b}, Trp^{59b}, Tyr^{62b}, Asp^{300b}, His^{305b}, Asp^{356}, Trp^{357}
FK	293.17	0.07455	F1, K2	Trp^{58b}, Trp^{59b}, Tyr^{62b}, His^{305b}
MR	305.15	0.02078	M1, R2	Trp^{58b}, Trp^{59b}, Tyr^{62b}, Asp^{300b}, His^{305b}
FFNSR	669.32	0.02173	F1, F2, N3, R5	Pro^{54}, Trp^{58b}, Trp^{59b}, Tyr^{62b}, Asp^{300b}, His^{305b}, Asp^{356}, Trp^{357}
WPDAR	643.31	0.006849	W1, P2, A4, R5	Phe^{17}, Trp^{58b}, Trp^{59b}, Tyr^{62b}, Asp^{96b}, Val^{98}, Arg^{195b}, Asp^{197b}, His^{299b}, Asp^{300b}, His^{305b}
LSGFPR	675.37	0.00394	L1, G3, F4, P5, R6	His^{15b}, Phe^{17}, Pro^{54}, Trp^{58b}, Trp^{59b}, Tyr^{62b}, Asp^{96b}, Arg^{195b}, His^{299b}, Asp^{300b}, His^{305b}, Asp^{356}, Trp^{357}
QFLR	562.32	0.0102	Q1, F2, L3, R4	Pro^{54}, Trp^{58b}, Trp^{59b}, Tyr^{62b}, His^{305b}, Asp^{356}, Trp^{357}
FLK	406.26	0.09452	F1, L2, K3	Phe^{17}, Trp^{58b}, Trp^{59b}, Tyr^{62b}, His^{299b}, Asp^{300b}, His^{305b}
AFPYK	624.33	0.005165	A1, F2, P3, Y4	Trp^{58b}, Trp^{59b}, Tyr^{62b}, Gln^{63}, Leu^{165}, Asp^{300b}, His^{305b}
F6				
FFK	440.24	0.04249	F1, F2, K3	Trp^{58b}, Trp^{59b}, Tyr^{62b}, Asp^{300b}, His^{305b}
SFR	408.21	0.05357	S1, F2, R3	Trp^{58b}, Trp^{59b}, Tyr^{62b}, Asp^{300b}, His^{305b}
CPPTPR	669.33	0.0003703	C1, P2, P3, P5, R6	His^{15b}, Phe^{17}, Pro^{54}, Trp^{58b}, Trp^{59b}, Tyr^{62b}, Asp^{96b}, Arg^{195b}, His^{299b}, Asp^{300b}, His^{305b}, Asp^{356}, Trp^{357}

Note:
[a] Binding site analysis by Pepsite 2 software (http://pepsite2.russelllab.org/).
[b] Binding residues on the AAM active sites.

Table 3
Bioactive peptide sequences and their interactions with potential DPP-IV binding sites.

Peptide sequence	Mw	Pepsite 2 (*p* value) [a]	Binding residues in peptide	Bound residues of DPP-IV
F4				
FR	322.19	0.005277	F1, R2	Tyr^{48}, Trp^{627}, Trp^{629b}, Gly^{741}, Tyr^{752}
WR	361.20	0.005748	W1, R2	Tyr^{48}, Trp^{627}, Trp^{629b}, Tyr^{752}
FGNWR	679.33	0.005428	G2, N3, W4, R5	Tyr^{48}, Trp^{627}, Trp^{629b}, His^{740b}, Gly^{741}, ILe^{742}, Ala^{743}, His^{748}, Tyr^{752}
MFK	425.22	0.003096	M1, F2, K3	Tyr^{48}, Trp^{627}, Trp^{629b}, Gly^{741}, Tyr^{752}
SFGPR	562.29	0.01877	G3, P4, R5	Phe^{357b}, Tyr^{547b}, Pro^{550}, Trp^{659b}, Tyr^{662b}, Asp^{663}, Tyr^{666b}, Thr^{667}, Tyr^{670}
NPPFK	601.32	0.0003259	P2, P3, F4, K5	Glu^{206b}, Phe^{357b}, Tyr^{547b}, Pro^{550}, Tyr^{662b}, Tyr^{666b}, Tyr^{670}
CPPSPR	655.31	0.1198	C1, P5, R6	Phe^{357b}, Tyr^{547b}, Pro^{550}, Trp^{629b}, Tyr^{666b}, Tyr^{670}, Tyr^{752}
DFR	436.21	0.02662	D1, F2, R3	Tyr^{48}, Trp^{627}, Trp^{629b}, His^{740b}, Gly^{741}, ILe^{742}, Ala^{743}, Tyr^{752}
FNFSR	669.32	0.007846	F1, N2, F3, R5	Phe^{357b}, Tyr^{547b}, Pro^{550}, Tyr^{631b}, Trp^{659b}, Tyr^{662b}, Asp^{663}, Tyr^{666b}, Thr^{667}, Tyr^{670}
LFFSR	668.36	0.0174	L1, F2, F3, R5	Tyr^{48}, Val^{546}, Trp^{627}, Gly^{628}, Trp^{629b}, Ser^{630b}, His^{740b}, Gly^{741}, Ile^{742}, Ala^{743}, Tyr^{752}
GFPSR	562.29	0.001407	F2, P3, S4, R5	Tyr^{48}, Trp^{627}, Trp^{629b}, His^{740b}, Gly^{741}, Ile^{742}, Ala^{743}, Tyr^{752}
FK	293.17	0.00525	F1, K2	Tyr^{48}, Trp^{627}, Trp^{629b}, Gly^{741}, Tyr^{752}
MR	305.15	0.00785	M1, R2	Trp^{629b}, Ser^{630b}, Gly^{741}, Tyr^{752}
FFNSR	669.32	0.005675	F2, N3, S4, R5	Tyr^{48}, Trp^{627}, Trp^{629b}, His^{740b}, Gly^{741}, ILe^{742}, Ala^{743}, Tyr^{752}
WPDAR	643.31	0.01173	W1, D3, A4, R5	Tyr^{48}, Trp^{627}, Trp^{629b}, His^{740b}, Gly^{741}, ILe^{742}, Ala^{743}, His^{748}, Tyr^{752}
LSGFPR	675.37	0.02638	L1, F4, P5, R6	Phe^{357b}, Val^{546}, Tyr^{547b}, Pro^{550}, Trp^{627}, Gly^{628}, Trp^{629b}, Ser^{630b}, Tyr^{631b}, Trp^{659b}, Tyr^{662b}, Asp^{663}, Tyr^{666b}, Thr^{667}, Tyr^{670}
QFLR	562.32	0.0202	Q1, F2, L3	Tyr^{48}, Trp^{627}, Trp^{629b}, Ser^{630b}, Val^{653}, Tyr^{752}
FLK	406.26	0.00615	F1, L2, K3	Tyr^{48}, Trp^{627}, Trp^{629b}, Tyr^{752}
AFPYK	624.33	0.0008243	A1, F2, P3, Y4	Tyr^{48}, Val^{546}, Trp^{627}, Gly^{628}, Trp^{629b}, Ser^{630b}, Gly^{741}, Tyr^{752}
F6				
FFK	440.24	0.003712	F1, F2, K3	Tyr^{48}, Trp^{627}, Trp^{629b}, Gly^{741}, Tyr^{752}
SFR	408.21	0.009356	S1, F2, R3	Tyr^{48}, Trp^{627}, Trp^{629b}, Tyr^{752}
CPPTPR	669.33	0.08718	T4, P5, R6	Tyr^{48}, Trp^{627}, Trp^{629b}, Tyr^{752}

Note:
[a] Binding site analysis by Pepsite 2 software (http://pepsite2.russelllab.org/).
[b] Binding residues on the DPP-IV active sites.

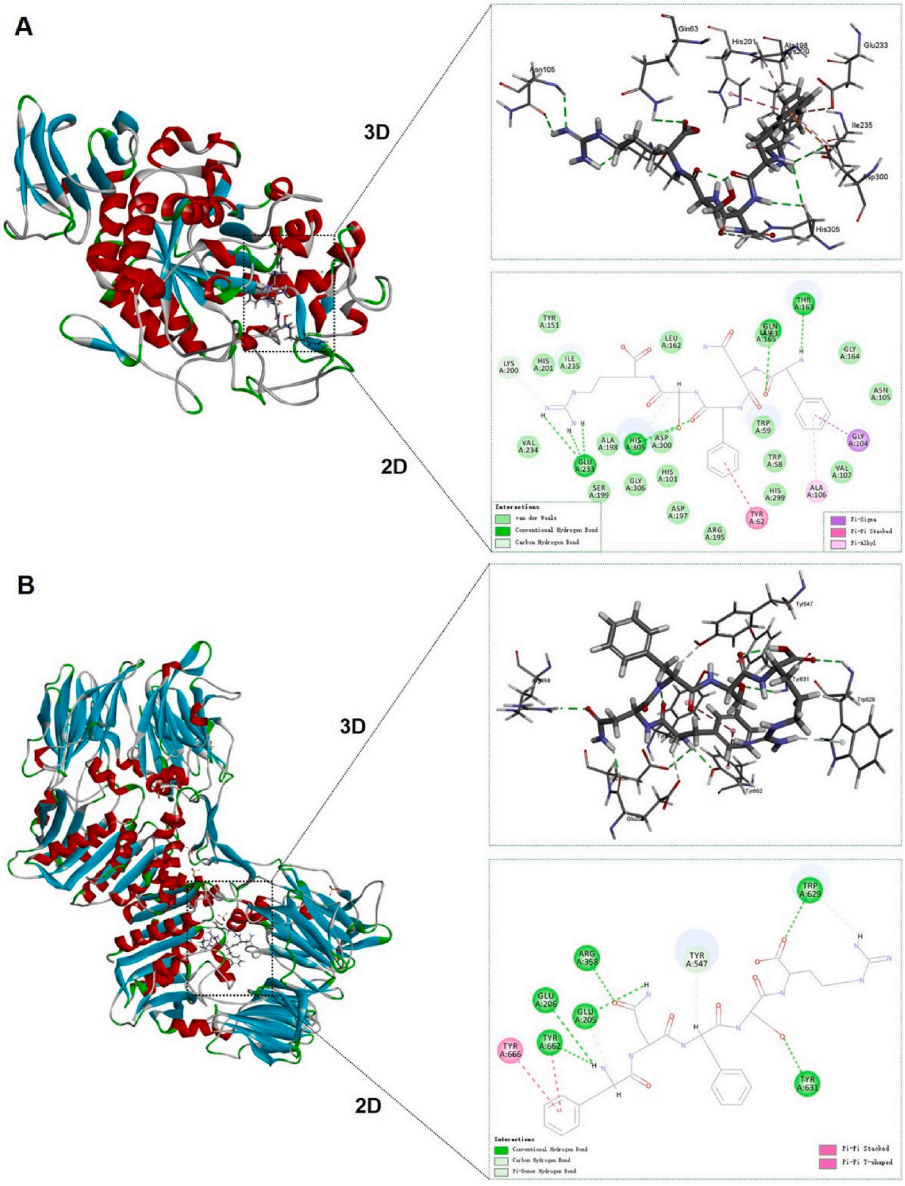

Fig. 6. Molecular docking of FNFSR to the target receptors of AAM and DPP-IV. (A) Binding mode between AAM (PDB code: 3BAJ) and FNFSR. (B) Binding mode between DPP-IV (PDB code: 4A5S) and FNFSR. The 3D structure represents the interaction in docking of the peptide FNFSR at AAM or DPP- IV active sites, and the 2D structure represents the way FNFSR binds to the amino acid residues of AAM or DPP- IV active sites.

of diabetic mice, reduce blood glucose levels and promote the recovery of insulin levels, resist the liver and kidney function damage caused by STZ, and protect liver, kidney and pancreatic tissues. The ultrafiltration fractions with higher inhibitory activity of α-amylase and DPP-IV were purified by gel filtration chromatography and RP-HPLC and identified by LC-ESI-Q-TOF-MS/MS. According to the results of bioinformatic analysis, a total of 37 and 4 potentially active peptide sequences were screened from the F4 and F6 fractions of TOH-2, respectively. Among them, 19 peptides in F4 and 3 peptides in F6 had significant antidiabetic potential, and could potentially bind the active sites of the target enzymes α-amylase and DPP- IV through binding within the internal cavity. Therefore, this study provides a possible strategy for the development of functional foods, dietary supplements, or pharmaceutical preparations for the prevention and/or treatment of T2DM by *T. ovatus* protein hydrolysates and their components. Moreover, as a protein-rich and underutilized marine fish, this study will promote future high value utilization.

CRediT authorship contribution statement

Peng Wan: Conceptualization, Methodology, Investigation, Software, Data curation, Writing – original draft, Visualization. **Bingna Cai:** Formal analysis, Validation. **Hua Chen:** Investigation, Validation. **Deke Chen:** Software, Formal analysis. **Xiangtan Zhao:** Software, Resources. **Huabiao Yuan:** Software, Validation. **Jingtong Huang:** Investigation, Data curation. **Xin Chen:** Writing – review & editing. **Lianxiang Luo:** Software. **Jianyu Pan:** Writing – review & editing, Supervision, Project administration, Funding acquisition.

Declaration of competing interest

The authors declare that they have no known competing financial interests or personal relationships that could have appeared to influence the work reported in this paper.

Data availability

Data will be made available on request.

Acknowledgments

The authors are indebted to Dr. Shikun Dai and Yongli Gao, and engineer Yun Zhang and Aijun Sun (the Equipment Public Service Center, SCSIO, CAS) for their assistance with the high-speed refrigerated centrifuge and mass spectrometric analysis. This research was supported by the Marine Economic Development Project (No. GDNRC [2022] 36), the Key-Area Research and Development Program of Guangdong Province (No. 2020B1111030004), the Institution of South China Sea Ecology and Environmental Engineering, Chinese Academy of Sciences (No. ISEE2021PY05), the Key Research and Development Program of Hainan Province (No. ZDYF2021SHFZ109), the National Natural Science Foundation of Guangdong (No. 2022A1515010767) and the Department of Education of Guangdong Province (2021KTSCX114).

Appendix A. Supplementary data

Supplementary data to this article can be found online at https://doi.org/10.1016/j.crfs.2023.100446.

References

Arunachalam, K., Parimelazhagan, T., 2013. Antidiabetic activity of ficus amplissima smith. Bark extract in streptozotocin induced diabetic rats. J. Ethnopharmacol. 147 (2), 302–310. https://doi.org/10.1016/j.jep.2013.03.004.

Auestad, N., Layman, D.K., 2021. Dairy bioactive proteins and peptides: a narrative review. Nutr. Rev. 79 (Suppl. ment_2), 36–47. https://doi.org/10.1093/nutrit/nuab097.

Awosika, T.O., Aluko, R.E., 2019. Inhibition of the in vitro activities of α-amylase, α-glucosidase and pancreatic lipase by yellow field pea (pisum sativum l.) protein hydrolysates. Int. J. Food Sci. Technol. 54 (6), 2021–2034. https://doi.org/10.1111/ijfs.14087.

Boachie, R.T., Okoro, F.L., Imai, K., Sun, L., Elom, S.O., Nwankwo, J.O., Ejike, C.E., Udenigwe, C.C., 2019. Enzymatic release of dipeptidyl peptidase-4 inhibitors (gliptins) from pigeon pea (cajanus cajan) nutrient reservoir proteins: in silico and in vitro assessments. J. Food Biochem. 43 (12), e13071 https://doi.org/10.1111/jfbc.13071.

Bunsroem, K., Prinyawiwatkul, W., Thaiudom, S., 2022. The influence of whey protein heating parameters on their susceptibility to digestive enzymes and the antidiabetic activity of hydrolysates. Foods 11 (6), 829. https://doi.org/10.3390/foods11060829.

Chalamaiah, M., Ulug, S.K., Hong, H., Wu, J., 2019. Regulatory requirements of bioactive peptides (protein hydrolysates) from food proteins. J. Funct.Foods 58, 123–129. https://doi.org/10.1016/j.jff.2019.04.050.

Deacon, C.F., Holst, J.J., 2006. Dipeptidyl peptidase iv inhibitors: a promising new therapeutic approach for the management of type 2 diabetes. Int. J. Biochem. Cell Biol. 38 (5–6), 831–844. https://doi.org/10.1016/j.biocel.2005.09.011.

Fowler, M.J., 2011. Microvascular and macrovascular complications of diabetes. Clin. Diabetes 29 (3), 116–122. https://doi.org/10.2337/diaclin.29.3.116.

Gao, L., Zhang, W., Yang, L., Fan, H., Olatunji, O.J., 2021. Stink bean (parkia speciosa) empty pod: a potent natural antidiabetic agent for the prevention of pancreatic and hepatorenal dysfunction in high fat diet/streptozotocin-induced type 2 diabetes in rats. Arch. Physiol. Biochem. 1–7 https://doi.org/10.1080/13813455.2021.1876733.

Harnedy-Rothwell, P.A., Khatib, N., Sharkey, S., Lafferty, R.A., Gite, S., Whooley, J., O'Harte, F.P., FitzGerald, R.J., 2021. Physicochemical, nutritional and in vitro antidiabetic characterisation of blue whiting (micromesistius poutassou) protein hydrolysates. Mar. Drugs 19 (7), 383. https://doi.org/10.3390/md19070383.

Harnedy, P.A., FitzGerald, R.J., 2012. Bioactive peptides from marine processing waste and shellfish: a review. J. Funct.Foods 4 (1), 6–24. https://doi.org/10.1016/j.jff.2011.09.001.

Harnedy, P.A., Parthsarathy, V., McLaughlin, C.M., O'Keeffe, M.B., Allsopp, P.J., McSorley, E.M., O'Harte, F.P., FitzGerald, R.J., 2018a. Atlantic salmon (salmo salar) co-product-derived protein hydrolysates: a source of antidiabetic peptides. Food Res. Int. 106, 598–606. https://doi.org/10.1016/j.foodres.2018.01.025.

Harnedy, P.A., Parthsarathy, V., McLaughlin, C.M., O'Keeffe, M.B., Allsopp, P.J., McSorley, E.M., O'Harte, F.P., FitzGerald, R.J., 2018b. Blue whiting (micromesistius poutassou) muscle protein hydrolysate with in vitro and in vivo antidiabetic properties. J. Funct.Foods 40, 137–145. https://doi.org/10.1016/j.jff.2017.10.045.

Hou, M., Xiang, H., Hu, X., Chen, S., Wu, Y., Xu, J., Yang, X., 2022. Novel potential xod inhibitory peptides derived from trachinotus ovatus: isolation, identification and structure-function analysis. Food Biosci. 47, 101639 https://doi.org/10.1016/j.fbio.2022.101639.

Huang, S.-L., Jao, C.-L., Ho, K.-P., Hsu, K.-C., 2012. Dipeptidyl-peptidase iv inhibitory activity of peptides derived from tuna cooking juice hydrolysates. Peptides 35 (1), 114–121. https://doi.org/10.1016/j.peptides.2012.03.006.

Inayati, A., Lee, B.-O., Wang, R.-H., Chen, S.-Y., Hsu, H.-C., Lu, C.-H., Lee, Y.-J., 2022. Determinants of fear of falling in older adults with diabetes. Geriatr. Nurs. 46, 7–12. https://doi.org/10.1016/j.gerinurse.2022.04.017.

Ishikawa, Y., Hira, T., Inoue, D., Harada, Y., Hashimoto, H., Fujii, M., Kadowaki, M., Hara, H., 2015. Rice protein hydrolysates stimulate GLP-1 secretion, reduce GLP-1 degradation, and lower the glycemic response in rats. Food Funct. 6 (8), 2525–2534. https://doi.org/10.1039/C4FO01054J.

Jensen, C., Dale, H.F., Hausken, T., Lied, E., Hatlebakk, J.G., Brønstad, I., Lied, G.A., Hoff, D.A.L., 2019. Supplementation with cod protein hydrolysate in older adults: a dose range cross-over study. J. Nutr. Sci. 8, e40. https://doi.org/10.1017/jns.2019.37.

Jonker, J., Wijngaarden, M., Kloek, J., Groeneveld, Y., Gerhardt, C., Brand, R., Kies, A., Romijn, J., Smit, J., 2011. Effects of low doses of casein hydrolysate on post-challenge glucose and insulin levels. Eur. J. Intern. Med. 22 (3), 245–248. https://doi.org/10.1016/j.ejim.2010.12.015.

Lacroix, I.M., Li-Chan, E.C., 2016. Food-derived dipeptidyl-peptidase IV inhibitors as a potential approach for glycemic regulation–current knowledge and future research considerations. Trends Food Sci. Technol. 54, 1–16. https://doi.org/10.1016/j.tifs.2016.05.008.

Liao, P.-Y., Lo, H.-Y., Liu, I.-C., Lo, L.-C., Hsiang, C.-Y., Ho, T.-Y., 2022. A gastro-resistant peptide from momordica charantia improves diabetic nephropathy in db/db mice via its novel reno-protective and anti-inflammatory activities. Food Funct. 13 (4), 1822–1833. https://doi.org/10.1039/D1FO02788C.

McLaughlin, C., Sharkey, S., Harnedy-Rothwell, P., Parthsarathy, V., Allsopp, P., McSorley, E., FitzGerald, R., O'Harte, F., 2020. Twice daily oral administration of palmaria palmata protein hydrolysate reduces food intake in streptozotocin induced diabetic mice, improving glycaemic control and lipid profiles. J. Funct.Foods 73, 104101. https://doi.org/10.1016/j.jff.2020.104101.

Mudgil, P., Kamal, H., Kilari, B.P., Salim, M.A.S.M., Gan, C.-Y., Maqsood, S., 2021. Simulated gastrointestinal digestion of camel and bovine casein hydrolysates: identification and characterization of novel anti-diabetic bioactive peptides. Food Chem. 353, 129374 https://doi.org/10.1016/j.foodchem.2021.129374.

Mudgil, P., Kilari, B.P., Kamal, H., Olalere, O.A., FitzGerald, R.J., Gan, C.-Y., Maqsood, S., 2020. Multifunctional bioactive peptides derived from quinoa protein hydrolysates: inhibition of α-glucosidase, dipeptidyl peptidase-IV and angiotensin I converting enzymes. J. Cereal. Sci. 96, 103130 https://doi.org/10.1016/j.jcs.2020.103130.

Nasri, R., Abdelhedi, O., Jemil, I., Daoued, I., Hamden, K., Kallel, C., Elfeki, A., Lamri-Senhadji, M., Boualga, A., Nasri, M., Châabouni, M.K., 2015. Ameliorating effects of goby fish protein hydrolysates on high-fat-high-fructose diet-induced hyperglycemia, oxidative stress and deterioration of kidney function in rats. Chem. Biol. Interact. 242, 71–80. https://doi.org/10.1016/j.cbi.2015.08.003.

Ngoh, Y.-Y., Gan, C.-Y., 2016. Enzyme-assisted extraction and identification of antioxidative and α-amylase inhibitory peptides from pinto beans (phaseolus vulgaris cv. Pinto). Food Chem. 190, 331–337. https://doi.org/10.1016/j.foodchem.2015.05.120.

Ngoh, Y.-Y., Gan, C.-Y., 2018. Identification of pinto bean peptides with inhibitory effects on α-amylase and angiotensin converting enzyme (ace) activities using an integrated bioinformatics-assisted approach. Food Chem. 267, 124–131. https://doi.org/10.1016/j.foodchem.2017.04.166.

Ngoh, Y.-Y., Lim, T.S., Gan, C.-Y., 2016. Screening and identification of five peptides from pinto bean with inhibitory activities against α-amylase using phage display technique. Enzym. Microb. Technol. 89, 76–84. https://doi.org/10.1016/j.enzmictec.2016.04.001.

Nong, N.T.P., Hsu, J.-L., 2021. Characteristics of food protein-derived antidiabetic bioactive peptides: a literature update. Int. J. Mol. Sci. 22 (17), 9508. https://doi.org/10.3390/ijms22179508.

Nongonierma, A.B., FitzGerald, R.J., 2014. Susceptibility of milk protein-derived peptides to dipeptidyl peptidase IV (DPP-IV) hydrolysis. Food Chem. 145, 845–852. https://doi.org/10.1016/j.foodchem.2013.08.097.

Nongonierma, A.B., FitzGerald, R.J., 2019. Features of dipeptidyl peptidase IV (DPP-IV) inhibitory peptides from dietary proteins. J. Food Biochem. 43 (1), e12451 https://doi.org/10.1111/jfbc.12451.

Phadke, G.G., Rathod, N.B., Ozogul, F., Elavarasan, K., Karthikeyan, M., Shin, K.-H., Kim, S.-K., 2021. Exploiting of secondary raw materials from fish processing industry as a source of bioactive peptide-rich protein hydrolysates. Mar. Drugs 19 (9), 480. https://doi.org/10.3390/md19090480.

Qin, Y., He, C., Geng, H., Wang, W., Yang, P., Mai, K., Song, F., 2022. Muscle nutritive metabolism changes after dietary fishmeal replaced by cottonseed meal in golden pompano (trachinotus ovatus). Metabolites 12 (7), 576. https://doi.org/10.3390/metabo12070576.

Ramírez Fuentes, L., Richard, C., Chen, L., 2021. Sequential alcalase and flavourzyme treatment for preparation of α-amylase, α-glucosidase, and dipeptidyl peptidase (dpp)-iv inhibitory peptides from oat protein. J. Funct.Foods 87, 104829. https://doi.org/10.1016/j.jff.2021.104829.

Ritian, J., Teng, X., Liao, M., Zhang, L., Wei, Z., Meng, R., Liu, N., 2021. Release of dipeptidyl peptidase iv inhibitory peptides from salmon (salmo salar) skin collagen based on digestion–intestinal absorption *in vitro*. Int. J. Food Sci. Technol. 56 (7), 3507–3518. https://doi.org/10.1111/ijfs.14977.

Sarteshnizi, R.A., Sahari, M.A., Gavlighi, H.A., Regenstein, J.M., Nikoo, M., Udenigwe, C. C., 2021. Influence of fish protein hydrolysate-pistachio green hull extract interactions on antioxidant activity and inhibition of α-glucosidase, α-amylase, and DPP-IV enzymes. LWT 142, 111019. https://doi.org/10.1016/j.lwt.2021.111019.

Shady, G., Rashwan, H.M., Althobaiti, F., Aldhahrani, A., Fayad, E., Shabana, E.-S., El-Hallous, E.I., Amen, R.M., 2022. Ad-mscs and bm-mscs ameliorating effects on the metabolic and hepato-renal abnormalities in type 1 diabetic rats. Saudi J. Biol. Sci. 29 (2), 1053–1060. https://doi.org/10.1016/j.sjbs.2021.09.067.

Siddik, M.A., Howieson, J., Fotedar, R., Partridge, G.J., 2021. Enzymatic fish protein hydrolysates in finfish aquaculture: a review. Rev. Aquacult. 13 (1), 406–430. https://doi.org/10.1111/raq.12481.

Somannavar, S., Ganesan, A., Deepa, M., Datta, M., Mohan, V., 2008. Random capillary blood glucose cut points for diabetes and pre-diabetes derived from community-based opportunistic screening in India. Diabetes Care 32 (4), 641–643. https://doi.org/10.2337/dc08-0403.

Soskolne, W.A., Klinger, A., 2001. The relationship between periodontal diseases and diabetes: an overview. Ann. Periodontol. 6 (1), 91–98. https://doi.org/10.1902/annals.2001.6.1.91.

Sun, H., Saeedi, P., Karuranga, S., Pinkepank, M., Ogurtsova, K., Duncan, B.B., Stein, C., Basit, A., Chan, J.C.N., Mbanya, J.C., Pavkov, M.E., Ramachandaran, A., Wild, S.H., James, S., Herman, W.H., Zhang, P., Bommer, C., Kuo, S., Boyko, E.J., Magliano, D. J., 2022. IDF Diabetes Atlas: global, regional and country-level diabetes prevalence estimates for 2021 and projections for 2045. Diabetes Res. Clin. Pract. 183, 109119 https://doi.org/10.1016/j.diabres.2021.109119.

Sun, J.L., Jiang, T., Gu, Y., Song, F.B., Wen, X., Luo, J., 2022. Differential immune and metabolic responses underlie differences in the resistance of siganus oramin and trachinotus blochii to cryptocaryon irritans infection. Fish Shellfish Immunol. 120, 166–179. https://doi.org/10.1016/j.fsi.2021.11.018.

Wan, P., Chen, D., Chen, H., Zhu, X., Chen, X., Sun, H., Pan, J., Cai, B.J.R.a., 2020. Hypolipidemic effects of protein hydrolysates from *trachinotus ovatus* and identification of peptides implied in bile acid-binding activity using LC-ESI-Q-TOF-MS/MS. RSC Adv. 10 (34), 20098–20109. https://doi.org/10.1039/D0RA02428G.

Wang, C., Zheng, L., Su, G., Zeng, X.-A., Sun, B., Zhao, M., 2020. Evaluation and exploration of potentially bioactive peptides in casein hydrolysates against liver oxidative damage in stz/hfd-induced diabetic rats. J. Agric. Food Chem. 68 (8), 2393–2405. https://doi.org/10.1021/acs.jafc.9b07687.

Wang, J., Wu, T., Fang, L., Liu, C., Liu, X., Li, H., Shi, J., Li, M., Min, W., 2020. Anti-diabetic effect by walnut (juglans mandshurica maxim.)-derived peptide lpllr through inhibiting α-glucosidase and α-amylase, and alleviating insulin resistance of hepatic hepg2 cells. J. Funct.Foods 69, 103944. https://doi.org/10.1016/j.jff.2020.103944.

Xiao, T., Zeng, J., Qiu, L., Wang, R., Li, N., Deng, Z., Zheng, L., 2022. Combining in silico and in vitro approaches to identify endogenous hypoglycemic peptides from human milk. Food Funct. 13 (5), 2899–2912. https://doi.org/10.1039/D1FO03537A.

Yu, Z., Yin, Y., Zhao, W., Liu, J., Chen, F., 2012. Anti-diabetic activity peptides from albumin against α-glucosidase and α-amylase. Food Funct. 135 (3), 2078–2085. https://doi.org/10.1039/D1FO03537A.

Zhao, W., Cui, X., Wang, Z.-Q., Yao, R., Chen, M.-D., Gao, B.-Y., Zhang, C.-W., Niu, J., 2022. Effects of barranca yajiagengensis powder in the diet of trachinotus ovatus on the growth performance, antioxidant capacity, immunity and morphology of the liver and intestine. Antioxidants 11 (7), 1220. https://doi.org/10.3390/antiox11071220.

Zhao, W., Zhang, D., Yu, Z., Ding, L., Liu, J., 2020. Novel membrane peptidase inhibitory peptides with activity against angiotensin converting enzyme and dipeptidyl peptidase IV identified from hen eggs. J. Funct.Foods 64, 103649. https://doi.org/10.1016/j.jff.2019.103649.

Zhou, M., Ren, G., Zhang, B., Ma, F., Fan, J., Qiu, Z., 2022. Screening and identification of a novel antidiabetic peptide from collagen hydrolysates of Chinese giant salamander skin: network pharmacology, inhibition kinetics and protection of IR-HepG2 cells. Food Funct. 13 (6), 3329–3342. https://doi.org/10.1039/D1FO03527D.